PHYSICAL REVIEW E **87**, 052801 (2013)

Horizontal visibility graphs generated by type-I intermittency

Ángel M. Núñez, Bartolo Luque, Lucas Lacasa, and Jose Patricio Gómez
Dept. Matemática Aplicada y Estadística, ETSI Aeronáuticos, Universidad Politécnica de Madrid, Madrid, Spain

Alberto Robledo
Instituto de Física y Centro de Ciencias de la Complejidad, Universidad Nacional Autónoma de México, Mexico
(Received 21 January 2013; published 9 May 2013)

The type-I intermittency route to (or out of) chaos is investigated within the horizontal visibility (HV) graph theory. For that purpose, we address the trajectories generated by unimodal maps close to an inverse tangent bifurcation and construct their associated HV graphs. We show how the alternation of laminar episodes and chaotic bursts imprints a fingerprint in the resulting graph structure. Accordingly, we derive a phenomenological theory that predicts quantitative values for several network parameters. In particular, we predict that the characteristic power-law scaling of the mean length of laminar trend sizes is fully inherited by the variance of the graph degree distribution, in good agreement with the numerics. We also report numerical evidence on how the characteristic power-law scaling of the Lyapunov exponent as a function of the distance to the tangent bifurcation is inherited in the graph by an analogous scaling of block entropy functionals defined on the graph. Furthermore, we are able to recast the full set of HV graphs generated by intermittent dynamics into a renormalization-group framework, where the fixed points of its graph-theoretical renormalization-group flow account for the different types of dynamics. We also establish that the nontrivial fixed point of this flow coincides with the tangency condition and that the corresponding invariant graph exhibits extremal entropic properties.

DOI: 10.1103/PhysRevE.87.052801 PACS number(s): 89.75.Hc, 05.45.Ac, 05.45.Tp

I. INTRODUCTION

One of the common transitions between regular and chaotic behavior is intermittency, the seemingly random alternation of long quasiregular or laminar phases, so-called intermissions, and relatively short irregular or chaotic bursts. Intermittency is omnipresent in nonlinear science and has been weighed against comparable phenomena in nature, such as Belousov-Zhabotinski chemical reactions, Rayleigh-Benard instabilities, turbulence, etc. [1–4]. The study and characterization of the onset mechanisms and main statistical properties of intermittency was carried out already a long time ago; Pomeau and Manneville [5] introduced a classification as types I–III for different kinds of intermittency. Subsequently, other types have been described and typified, such as on-off intermittency [6], ring intermittency [7], etc. Our objective here is to generate networks from the time series associated with intermittency and look at how this phenomenon translates into such a different setting, and then examine the manifestation of its properties in the new context. For definiteness we chose the case of type-I intermittency as it occurs just preceding an (inverse) tangent bifurcation in nonlinear iterated maps, although the very same methodology can be extended to other situations. Specifically, we show how this phenomenon can be visualized through the graphs generated when the horizontal visibility (HV) algorithm [8–10] is applied to the trajectories of the universality class of unimodal maps, as represented by the quadratic logistic map.

The idea of mapping time series into graphs is actively developed at present via different approaches [8,9,11–17]. Amongst them, the HV approach offers a promising new method for performing time series analysis, most of all because it has been corroborated that the fundamental nature of rather different complex dynamical processes is inherited by the associated visibility graphs. As part of the effort of developing a mathematically sound visibility graph theory of dynamical systems, in recent years the performance of the visibility method has been tested and found to be consistently capable in different circumstances, including the description of chaotic, fractal-stochastic, dissipative processes [18,19]. The method has also been successfully applied in the characterization of real-world time series in different fields such as physiology and geophysics to cite some [20–23]. In every case the network counterpart of each particular kind of dynamics has been determined with precision, positioning the visibility algorithm as a well-defined method to analyze the dynamics of complex systems using graph-theoretical tools. In the context of low-dimensional chaos, two main routes to chaos have been studied in the light of this technique. Specifically, the period-doubling bifurcation cascade (Feigenbaum scenario) and the quasiperiodic route have been analyzed through the HV formalism and two complete sets of graphs, called Feigenbaum and quasiperiodic graphs, respectively, that encode the dynamics of their corresponding classes of iterated maps, have been introduced and characterized recently [24–27]. The third well-known route to chaos present in low-dimensional dissipative systems is type-I intermittency (Pomeau-Manneville scenario), and in the present work we present the structural, scaling, and entropic properties of the graphs obtained when the HV formalism is applied to this situation.

Before proceeding, let us briefly discuss some general issues and motivations concerning this particular method. Once the HV procedure was envisaged and proposed [9], a first task was to investigate whether the transformation is well defined and that the patterns present in the time series are properly reflected in graph space. In general, this is a huge task since the range of possible dynamical behaviors to be addressed is vast, and in the past years we have focused, in order to validate the method, on some of the most representative ones (periodic,

random, chaotic, fractal, etc.). We have found that the kernel dynamics in each case is well captured by the associated graphs (in some cases very easily when compared to traditional methods; see, for instance, the case of discriminating chaos from stochasticity [18]). It is also worth noticing that when the HV method is applied to a time series of unknown source, inspection of the resulting graph provides basic information about its nature, i.e., its underlying dynamics, and without referral to paradigmatic systems. To cite some examples, for a process with unknown detailed dynamics the HV method indicates whether it is statistically reversible (a stationary steady state in thermodynamical equilibrium with a thermal bath) or, on the contrary, statistically irreversible and dissipative, without the need to make an *ad hoc* symbolization of the series [19]. Also, in a system whose dynamics is unknown the HV method can distinguish periodic dynamics polluted with noise from chaotic dynamics within an attractor divided into bands, when the correlation function fails to differentiate between the two options [28]. Finally, a time series can be determined via the HV method to be random or chaotic without knowing where it comes from [9,18]. Also note that the HV method distills time series, condensing classes of them into a single graph that represents their basic common properties (e.g., a periodic time series leads always to a periodic network with motifs that portray the essentials of the periodicity that is being analyzed, and similarly with quasiperiodic and chaotic time series). That is, the method uncovers structural features, and forms sets of time series with the same feature by their representative HV graph, excluding from the group those that lack that feature. In this sense the HV method is not invertible, like other important tools, such as the renormalization-group and symbolic dynamics methods. While this noninvertibility can be recovered by appropriately weighting the resulting graph [9], we recall that the aim of the method is precisely to characterize and gather together series with analogous dynamics, rather than find graph analogues of single time series.

In the following, we first recall in Sec. II the key aspects of type-I intermittency. In Sec. III we present the horizontal visibility algorithm and apply it to the study of trajectories generated by unimodal maps close to an inverse tangent bifurcation, where type-I intermittency takes place. A phenomenological derivation of the degree distribution $P(k;\epsilon)$ of this kind of graph is performed. We show that this single graph metric encodes the key scaling properties of type-I intermittency, namely (i) the mean length $\langle \ell \rangle$ of the laminar episodes with ϵ manifests in network space as a comparable scaling with the same variable of the second moment $\langle k^2 \rangle$ of the degree distribution $P(k,\epsilon)$, and (ii) the scaling of Lyapunov exponent $\lambda(\epsilon)$ is recovered in network space from the Shannon block entropies over $P(k;\epsilon)$.

Next, in Sec. IV we recast the family of HV graphs generated by intermittent series into a graph-theoretical renormalization-group (RG) framework and determine the RG flows close to and at tangency. We show that there are two trivial fixed points akin to the high- and low-temperature fixed points in thermal phase transitions together with a nontrivial fixed point associated with the tangency condition. Finally, we also determine the extremal entropic properties of the RG fixed points as well as the entropy evolution along the RG flows.

II. TYPE-I INTERMITTENCY

Type-I intermittency can be observed infinitely many times in the logistic map

$$x_{t+1} = F(x_t) = \mu x_t(1 - x_t), \quad 0 \leqslant x \leqslant 1, \quad 0 \leqslant \mu \leqslant 4, \tag{1}$$

close to the control parameter values $\mu = \mu_T$ at which windows of periodicity open with period T for values $\mu > \mu_\infty \simeq 3.569\,945\,672\ldots$, where μ_∞ is the accumulation point of the main period-doubling cascade that locates the first appearance of chaos when increasing μ from small values. It can be observed that at $\mu_3 = 1 + \sqrt{8}$ this map exhibits a cycle of period $T = 3$ with subsequent bifurcations. This is the most visible window of periodicity in the chaotic regime and the one in whose vicinity our simulations have been performed. The regular periodic orbits hold slightly above μ_T, but below μ_T the dynamics consists of laminar episodes interrupted by chaos, a phenomenon known as intermittency. In what follows we relabel $\mu_T \equiv \mu_c$ and define $\epsilon \equiv \mu_c - \mu$. In the upper part of Fig. 1 we show a sample type-I intermittent time series generated by the logistic map close to μ_3, showing alternation between laminar trends, represented by black dots in the series, and chaotic bursts, represented in turn by white dots. We note that the laminar phase is not actually periodic, but approaches a periodic behavior of period 3 and it is precisely this behavior which is close to periodicity that makes it easily distinguishable from the chaotic bursts.

A. Basic properties of intermittent series generated by unimodal maps

Under rather general circumstances, trajectories generated by canonical models evidencing type-I intermittency show power-law scaling in the mean length of laminar phases

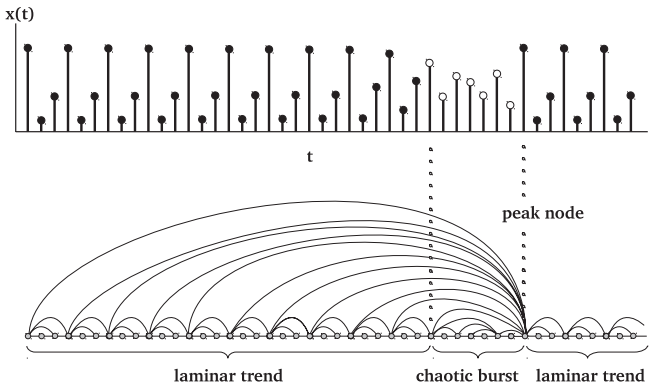

FIG. 1. Graphical illustration of how the horizontal visibility (HV) graph inherits in its structure the dynamics of the associated intermittent series. In the top of the figure we show a sample intermittent series generated by the logistic map close to μ_c ($\epsilon > 0$), producing laminar regions (black) mixed with chaotic bursts (white). In the bottom we plot the associated HV graph. Laminar regions are mapped into nodes with a periodic backbone, whereas the actual pseudoperiodicity of the series is inherited in the graph by the existence of so-called peak or interfacial nodes. Chaotic bursts are mapped into chaotic nodes, with a characteristic degree distribution (see the text).

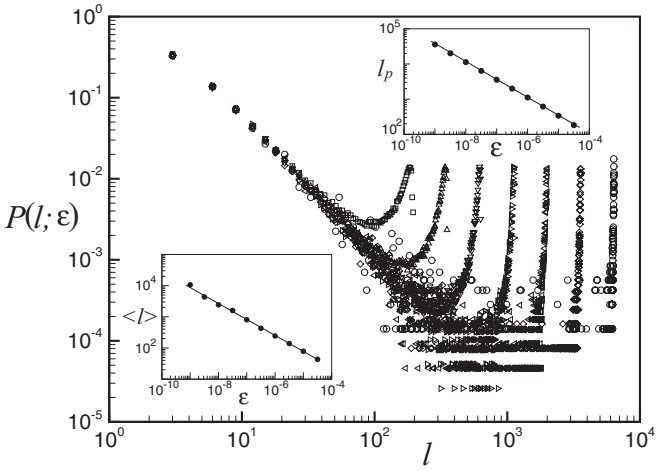

FIG. 2. Log-log plot of the length distribution of laminar phases $P(\ell;\epsilon)$ in our system, derived numerically from time series of 10^7 data generated through the logistic map (all over the work numerical analysis is performed over time series of similar size), or different values of ϵ: (squares) $\epsilon = 3 \times 10^{-5}$, (up triangles) $\epsilon = 10^{-5}$, (down triangles) $\epsilon = 3 \times 10^{-6}$, (right triangles) $\epsilon = 10^{-6}$, (left triangles) $\epsilon = 3 \times 10^{-7}$, (diamonds) $\epsilon = 10^{-7}$, and (circles) $\epsilon = 3 \times 10^{-8}$. The starting power-law decay is saturated at certain lengths, obtaining the classical asymmetrical U-shaped curves. (Inset bottom panel) Log-log plot of the laminar phases mean length $\langle \ell \rangle$ as a function of ϵ, yielding the expected scaling $\langle \ell \rangle \sim \epsilon^{-0.5}$. (Inset upper panel) Log-log plot of the local maximum of the distribution l_p as a function of ϵ, also yielding a scaling $l_p \sim \epsilon^{-0.5}$.

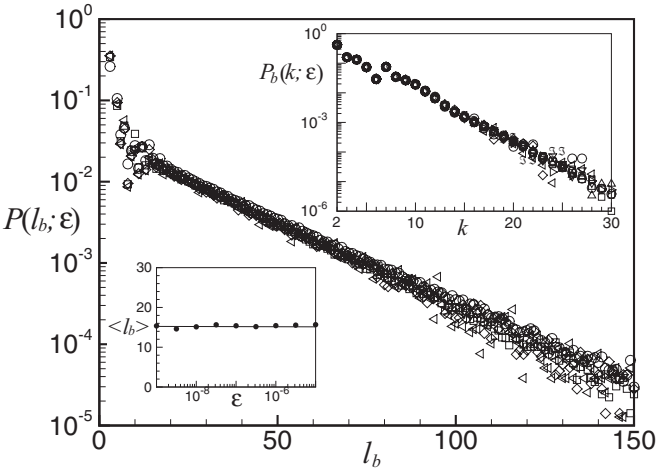

FIG. 3. Semilog plot of the size distribution of chaotic bursts in the system, showing a clear exponential decay which is fairly independent of ϵ. This behavior, which can be understood as a result of the survival time of an random uncorrelated process, suggests that the relaminarization process occurs at unpredictable, uncorrelated times. (Inset bottom panel) Mean length of the chaotic bursts $\langle l_b \rangle$ for different values of ϵ, showing a constant value $\langle l_b \rangle \approx 15$. (Inset upper panel) Semilog plot of the degree distribution associated to the nodes belonging to chaotic bursts $P_b(k)$, for different values of ϵ. The exponential decay, characteristic of an HV graph associated to a chaotic series, has been already found in several other maps [9,18]. The results seem to be independent of ϵ, in good agreement with the fact that the relaminarization process occurs at unpredictable times, which suggests $P_b(k) = A \exp(-ck)$.

$\langle \ell \rangle \sim \epsilon^{-\gamma}$, where ϵ, called the channel width of the Poincaré section, is the distance between the local Poincaré map and the diagonal [29]. The specific value of exponent γ is typically associated to the reinjection mechanism and several exponents have been reported, although $\gamma = 0.5$ holds in a rather large set of situations [30]. In Fig. 2 we plot in log-log scales the size distribution of laminar phases $P(\ell;\epsilon)$, derived numerically from time series of 10^7 data generated through the logistic map, for different values of ϵ, showing the characteristic asymmetric U shape. In the bottom inset panel of the same figure, we plot the dependence of the mean length of laminar trends with ϵ, showing the well studied scaling $\langle \ell \rangle \sim \epsilon^{-1/2}$. We finally note that the maximum length of the laminar trends ℓ_p, the extremum of the distribution $P(\ell;\epsilon)$, scales also as $\ell_p \sim \epsilon^{-1/2}$.

On the other hand, the length of a chaotic burst is known to be unpredictable. In Fig. 3 we plot, in semilog scales, the size distribution of chaotic bursts $P(\ell_b;\epsilon)$ for the same time series as used in Fig. 2. This distribution has in turn an exponential decay which becomes fairly independent of ϵ for sufficiently large lengths, a result that can be justified invoking the survival time of a random memoryless process. In the lower inset of Fig. 3 we numerically check that, as $P(\ell_b;\epsilon) \approx P(\ell_b)$, the mean length of the chaotic bursts remains constant independent of ϵ, with an approximated value of $\langle \ell_b \rangle \approx 15$.

III. TRANSFORMATION OF INTERMITTENT TIME SERIES INTO HORIZONTAL VISIBILITY GRAPHS

The horizontal visibility (HV) algorithm [8,9] assigns each datum x_i of a time series $\{x_i\}_{i=1,2,\ldots}$ to a node i in its associated HV graph (HVg), where i and j are two connected nodes if $x_i, x_j > x_n$ for all n such that $i < n < j$. Structural properties of a time series are inherited by its HVg (see the Appendix for some specific properties relevant to the intermittent structure). In the bottom part of Fig. 1 we show the HV graph of the associated intermittent series, which consists of several repetitions of a three-node motif (periodic backbone) linked to the first node of the subsequent laminar trend, interwoven with groups of nodes irregularly (chaotically) connected amongst them. We observe that the motif repetitions in the graph correspond to the laminar regions in the trajectory (pseudoperiodic data with pseudoperiod 3) and the chaotically connected groups correspond to the chaotic bursts in the trajectory. As laminar trends are indeed pseudoperiodic in the sense that they can be decomposed as a periodic signal and a drift (see the Appendix), this pseudoperiodicity expresses in the graph structure by allowing a node for each period-3 motif to be connected to the first node in the next laminar region (the so-called peak or interfacial node), as the values of the time series in the chaotic bursts are always smaller than those in the former laminar trend. The sequence of degrees is of the form 2-3-6 for laminar trends and loses this pattern in the chaotic burst. At odds with standard approaches, for which the distinction between laminar and chaotic phases is somewhat ambiguous, in this work we take advantage of this characteristic pattern as the criterion to numerically distinguish between both phases.

The assembly of repeated three-node motifs separated by sets of nodes with chaotic links inherited by the HVg from

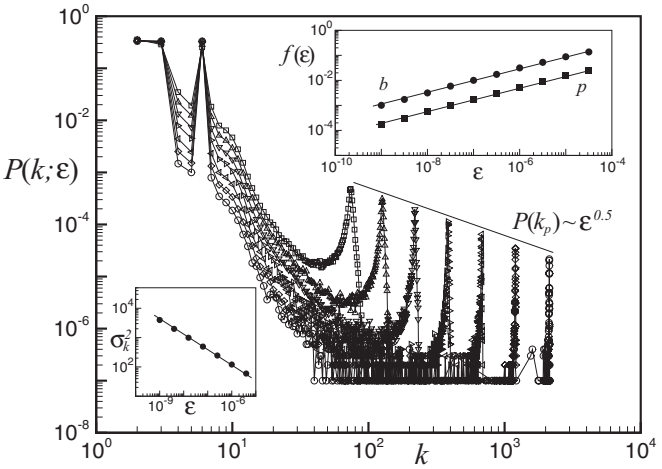

FIG. 4. Log-log plot of the total degree distribution $P(k;\epsilon)$ of 7 HV graphs mapped from trajectories of the logistic map in the vicinity of the window of period 3 ($\epsilon > 0$). Squares: $\epsilon = 3 \times 10^{-5}$; up triangles: $\epsilon = 10^{-5}$; down triangles: $\epsilon = 3 \times 10^{-6}$; right triangles: $\epsilon = 10^{-6}$; left triangles: $\epsilon = 3 \times 10^{-7}$; diamonds: $\epsilon = 10^{-7}$; circles: $\epsilon = 3 \times 10^{-8}$. Note that the tail of each distribution, associated to the peak nodes, scales with $\epsilon^{0.5}$, while this scaling is absent in the tail of the peak degree distribution (see the main panel of Fig. 5). This scaling is reminiscent of the contribution of the amount of peak nodes present in each series, whose abundance scales with $\epsilon^{0.5}$ (see the inset upper panel of this figure). (Inset upper panel) Log-log plot of the fraction of nodes associated with chaotic bursts, showing a scaling $f_b(\epsilon) \simeq 54\epsilon^{0.5}$ (circles), and fractions of peak (interfacial) nodes, showing a scaling $f_p(\epsilon) \simeq 3.2\epsilon^{0.5}$ (squares). (Inset bottom panel) Log-log plot of the variance of the total degree distribution $\sigma_k^2 = \langle k^2 \rangle - \langle k \rangle^2$ as a function of ϵ, obtained from the same graphs whose degree distribution is plotted in the main panel. A power-law scaling of the form $\sigma_k^2 \sim \epsilon^{-0.5}$ is found, which is the graph analog of the well-known laminar phase scaling reported in the inset bottom panel of Fig. 2.

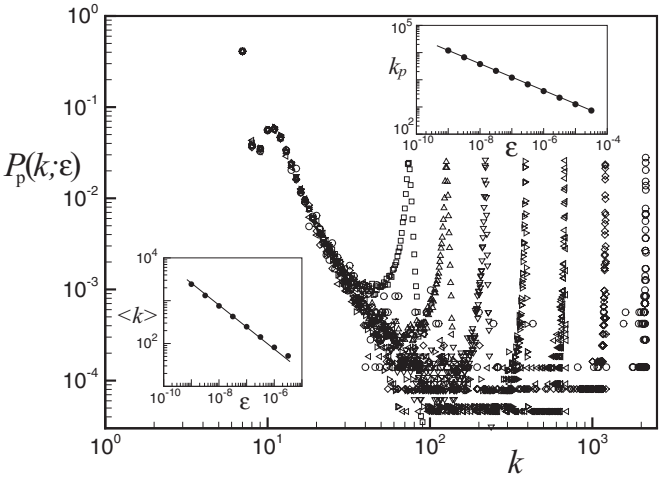

FIG. 5. Log-log plot of the degree distribution of the so-called peak nodes, obtained from the HV graphs at different values of ϵ. The asymmetrical U shape is qualitatively similar to the size distribution of laminar phases (see the text). (Inset bottom panel) Log-log plot of the mean degree of peak nodes, as a function of ϵ, calculated from the distributions plotted in the main panel of the figure. The scaling coincides with $\langle \ell \rangle/3$ (see the text). (Inset upper panel) Log-log plot of the local maximum of the distribution k_p as a function of ϵ showing a scaling $k_p \sim \epsilon^{-0.5}$.

the laminar trends and chaotic bursts in the intermittent series leaves also a characteristic footprint in its degree distribution $P(k;\epsilon)$ (see Fig. 4). This can be seen when $P(k;\epsilon)$ is compared with that for fully chaotic motion (see, for instance, [18]). In the former the connectivity of the nodes in the three-node motifs is over-represented than in the latter, since their relative frequencies are proportional to the length of the laminar episodes. Also, nodes with large degree (peak or interfacial nodes), increasingly large as ϵ decreases, emerge due to reinjections after chaotic bursts because these have visibility over the nodes from laminar phases. The evidence collected leads us to express the total degree distribution $P(k;\epsilon)$ as composed of three contributions that originate from three different types of nodes. Namely, the following.

(i) Laminar. The contribution from the laminar phases, $P_l(k;\epsilon)$, consists of a discrete set of degrees that corresponds to the background periodic behavior. By construction (see the Appendix) a periodic series with a superimposed drift generates a graph where the nodes have, for the particular case in which $T = 3$, a degree belonging to the set $\{2,3,6\}$; therefore, $P_l(k;\epsilon) \equiv P_l(k) = 1/3$ when $k = 2,3,6$, and zero otherwise.

(ii) Chaotic. The contribution from the chaotic bursts, $P_b(k;\epsilon)$, which, according to previous works [9,18], has an exponential decay (see the upper inset panel of Fig. 3 for numerical evidence). Moreover, as argued in the previous section, since the mean size of chaotic bursts is independent of ϵ (as we can see in the inset bottom panel of Fig. 3), the contribution $P_b(k;\epsilon)$ is thus also independent of ϵ, and in general reads $P_b(k;\epsilon) = P_b(k) \sim \exp(-ck)$, where the specific value of c depends on the chaos dimensionality [18].

(iii) Peak. The contribution from the interface between the chaotic and laminar phases, $P_p(k;\epsilon)$ (see Fig. 5), arises from the peak nodes, with a very large degree that is approximately proportional to the size of the laminar phase. Roughly, all of the peak nodes inherit a degree based on their visibility of the previous laminar phase, and therefore we *a priori* may assume that $P_p(k;\epsilon) \approx P(\ell/3;\epsilon)$ (see Figs. 2 and 5). The factor of $1/3$ arises because, for the periodic window studied, $k \sim \ell/3$ (or $k \sim \ell/T$ if the study focuses on intermittency close to a periodic window of period T), as we can observe in Fig. 1. In particular, the maximum laminar size and peak node degree scale similarly, $\ell_p/3 \approx k_p \sim \epsilon^{-0.5}$ (see the upper panels of Figs. 2 and 5). Note, however, that the connectivity k of the peak nodes is not straightforwardly distributed as ℓ, since the actual value of the degree of the peak node assigned by the HV is not necessarily equal to the size of the full laminar phase, but varies somewhat according to the actual value (position) of the series datum at reinjection (compare Figs. 5 and 2). That is to say, visibility of a peak node may be as large as the preceding laminar trend, but it can also be smaller if reinjection takes place below tangency, or larger, allowing full visibility of the preceding trend and part of the previous one, if reinjection takes place above tangency.

Nevertheless, in the following we will argue, and have numerically checked, that $P_p(k;\epsilon)$ and $P(\ell/3;\epsilon)$ have, up to first order, similar first and second moments, concretely. (a) The mean degree of peak nodes is approximately equal to 1/3 the mean value of the laminar phase size. This is due to the fact that the degree of peak nodes statistically *self-averages* over laminar phase sizes, as the variability in reinjection is symmetrical with respect to tangency. And (b) the second moment of $P_p(k;\epsilon)$ is associated with both the second moment of $P(\ell;\epsilon)$ and the variance of the reinjection distribution. However, the contribution of the latter is typically much smaller than the former. Indeed, whereas fluctuations in the reinjection position tend to decrease as ϵ decreases, fluctuations in the size of laminar trends tend to increase as ϵ decreases (this has been confirmed numerically). Therefore, the leading contribution comes from the variability of laminar sizes for small values of ϵ.

The aforementioned phenomenology lead us to formally write down $P(k;\epsilon)$ as

$$P(k;\epsilon) = f_l(\epsilon)P_l(k) + f_b(\epsilon)P_b(k) + f_p(\epsilon)P_p(k;\epsilon), \qquad (2)$$

where $f_l(\epsilon), f_b(\epsilon)$, and $f_p(\epsilon)$ are the fractions of nodes in the graph that correspond to laminar, chaotic, and peak regions, respectively. In order to derive these fractions, we rely on three restrictions, namely as follows.

(i) *Normalization,* which trivially implies $f_l(\epsilon) + f_b(\epsilon) + f_p(\epsilon) = 1$.

(ii) *Bounded degree.* It has been proved [9,24,25] that aperiodic series generate an HVg with constant mean degree $\langle k\rangle = 4$, the upper bound value for HV graphs. This restriction implies

$$f_l(\epsilon)\sum_k k P_l(k) + f_b(\epsilon)\sum_k k P_b(k) + f_p(\epsilon)\sum_k k P_p(k;\epsilon) = 4. \qquad (3)$$

Note that, in the latter expression, the first sum is trivially $\sum_k k P_l(k) = 11/3$, the second sum corresponds to the graph associated with a chaotic series, and is directly $\sum_k k P_b(k) = 4$ [24,25], while the third sum yields, due to the aforementioned arguments, $\sum_k k P_p(k;\epsilon) \approx \langle\ell\rangle/3$.

(iii) After each chaotic burst a peak node emerges and anticipates the next laminar region, what implies $f_b = f_p\langle\ell_b\rangle$, where $\langle\ell_b\rangle$ is the mean size of a chaotic burst and has been argued to be ϵ independent.

After a little algebra, (i), (ii), and (iii) along with the rest of the arguments yield the prediction $\langle\ell_b\rangle = 11$, $f_b = 11 f_p$, $f_l = 1\text{–}12 f_p$, and $f_p = \langle\ell\rangle^{-1}$.

In order to compare our phenomenological prediction with the numerics, we recall that under rather general conditions $\langle\ell\rangle \approx 0.2\epsilon^{-0.5}$ [31], which indeed coincides with the scaling plotted in the lower inset panel of Fig. 2. The predicted values for the fractions are therefore $f_p = 5\epsilon^{0.5}$, $f_b = 55\epsilon^{0.5}$, and $f_l = 1\text{–}60\epsilon^{0.5}$. These can be compared with the results of numerical simulations, shown in the upper inset panel of Fig. 4, for which the best fit are $f_p \approx 3.2\epsilon^{0.5}$, $f_b \approx 54\epsilon^{0.5}$, $f_l \approx 1\text{–}57.2\epsilon^{0.5}$, and additionally $\langle\ell_b\rangle \approx 15$ (bottom inset panel of Fig. 3), on fairly good agreement with our prediction. To give a hint of the statistics available in our numerics, note that for a time series of 10^7 data, the number of peak events for the lowest value of ϵ explored, $\epsilon = 3\times10^{-8}$, is no. events $= 10^7 f_p \approx 5\times10^3$.

A. Variance $\sigma_k^2 = \langle k^2\rangle - \langle k\rangle^2$: Graph analog of $\langle\ell\rangle$

While there can be no equivalence between $\langle\ell\rangle$ and $\langle k\rangle$ in the intermittent graphs as the latter is fixed to be $\langle k\rangle = 4$ for an aperiodic regime [19], a relationship may hold between $\langle\ell\rangle$ and higher moments of $P(k;\epsilon)$. Note that there is an increasing dispersion of the values of k from its mean $\langle k\rangle$ in the degree distributions of the graphs as $\epsilon \to 0^+$, that we show below is related to the distribution connectivity $P_p(k;\epsilon)$. If we measure this dispersion by means of the variance of the total degree distribution $\sigma_k^2 = \langle k^2\rangle - \langle k\rangle^2$ we recover numerically the $\epsilon^{-0.5}$ scaling, as shown in the bottom inset panel of Fig. 4.

This scaling is also a prediction of our phenomenological theory:

$$\sigma_k^2 = \langle k^2\rangle - \langle k\rangle^2 = f_l(\epsilon)\sum_k k^2 P_l(k) + f_b(\epsilon)\sum_k k^2 P_b(k) + f_p(\epsilon)\sum_k k^2 P_p(k;\epsilon) - \langle k\rangle^2. \qquad (4)$$

Proceeding as before, the first sum is $\sum_k k^2 P_l(k) = 49/3$ and the second sum $\sum_k k^2 P_b(k)$ is finite and ϵ independent. To determine the third sum we recall that the variance of the distributions $P_p(k;\epsilon)$ and $P(\ell;\epsilon)$ are equal up to first order in ϵ^{-1} (the variance associated with the reinjection probability is always a smaller quantity), yielding $\sum_k k^2 P_p(k;\epsilon) \sim \sum_\ell \ell^2 P(\ell;\epsilon) \sim \epsilon^{-1}$, where the higher-order terms take into account the fluctuations associated to the reinjection variability. Collecting these results we straightforwardly find

$$\sigma_k^2 \sim \epsilon^{-0.5}, \qquad (5)$$

for small values of ϵ. This is a main quantitative result linking the key property of intermittent time series with its counterpart in the corresponding HV graphs.

To round off, we here provide as an ansatz a concrete expression for $P_p(k;\epsilon)$:

$$P_p(k;\epsilon) \sim k^{-\alpha}\frac{\epsilon^{\alpha/2}}{|k-k_p|+1}, \qquad (6)$$

where $k_p = a\epsilon^{-0.5}$. This ansatz complies with all the properties obtained in our phenomenological theory (although note that we do not need to use it to derive several observables as the fraction of nodes or the variance σ_k^2), and provide a closed expression for the total degree distribution. This closed expression allows us to calculate the concrete degree distribution at tangency. This consists of an infinite-size laminar phase and a "phantom" of k_p with diverging degree and vanishing probability of occurrence. Incidentally, note that in this limit case we also recover $\langle k\rangle = \sum k P(k;\epsilon\to 0) = 4$, as expected.

B. Scaling of Lyapunov exponent: Block entropies h_n

In the previous section we have studied how the scaling of $\langle l\rangle$ was inherited in $P(k)$ by k_p and σ_k^2, but there exists another well-known scaling relation in the type-I intermittency route

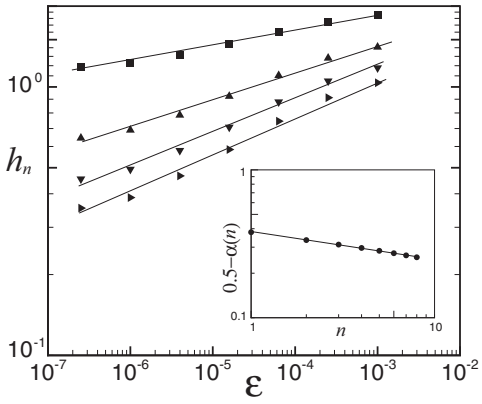

FIG. 6. Log-log plot of the block entropies h_n constructed from degree distributions of n sequence of connectivities in the HV graphs as a function of ϵ: $n = 1$ (squares), $n = 2$ (up triangles), $n = 3$ (down triangles), and $n = 4$ (right triangles). A scaling of the form $h_n \sim \epsilon^{\alpha(n)}$, reminiscent of the well-known scaling of the Lyapunov exponent $\lambda \sim \epsilon^{0.5}$ is found, albeit with a different, n-dependent exponent $\alpha(n)$. (Inset panel) Log-log plot of the convergence of $\alpha(n)$ to the exponent associated to the Lyapunov exponent, as a function of n. A relation of the form $[0.5 - \alpha(n)] \sim n^{-0.19}$ is found, whose extrapolation suggests $\lim_{n\to\infty} \alpha(n) = 0.5$.

involving the Lyapunov exponent

$$\lambda = \lim_{n\to\infty} \frac{1}{n} \sum_{i=0}^{n-1} \ln |F'(x_i)| \tag{7}$$

of the trajectories [5], which reads $\lambda \sim \epsilon^{0.5}$ as $\epsilon \to 0$. We recall here that the Pesin identity relates the positive Lyapunov exponents of a chaotic dynamics with the Kolmogorov-Sinai entropy of the system. In recent works [24,25,27], such a relation has been investigated in the visibility graph framework, through the definition of a graph-theoretical entropy, a Shannon-like entropy over the degree distribution

$$h_1 = -\sum_k P(k) \log P(k). \tag{8}$$

In Fig. 6 we plot in log-log the values of h_1 (solid squares) as a function of the channel width ϵ. A power-law scaling is recovered, albeit with a different scaling exponent $\alpha < 0.5$. Notice, however, that h_1 is only a proxy of the Kolmogorov-Sinai entropy and thus a comparison with the Lyapunov exponent is only approximate. Interestingly, h_1 is indeed the graph-theoretical version of a size-1 block entropy over the degree distribution. Since the Kolmogorov-Sinai entropy of a map can be recovered as the asymptotic limit of block entropies [32,33] $s(n) = -\frac{1}{n} \sum_{x_1,\ldots,x_n} p(x_1, \ldots, x_n) \log p(x_1, \ldots, x_n)$, we take advantage of this fact to define a set of graph-theoretical block entropies,

$$h_n = -\frac{1}{n} \sum_{k_1,\ldots,k_n} P(k_1, \ldots, k_n) \log P(k_1, \ldots, k_n). \tag{9}$$

The ϵ dependence of these block entropies is also plotted in Fig. 6, for different block sizes n. We observe in every case a power-law scaling $h_n \sim \epsilon^{-\alpha(n)}$. In the inset of the same figure we show how the exponent $\alpha(n)$ converges with n to the exponent found for the scaling of the Lyapunov exponent, suggesting

$$\lim_{n\to\infty} h_n = \lambda. \tag{10}$$

We remark at this point that, whereas the entropy is a magnitude defined in the graph, the Lyapunov exponent is only defined in the system. Therefore, in rigor the Pesin identity cannot be used here as the explanation for Eq. (10), as we are mixing properties defined in two different contexts. However, the strong numerical evidence in favor of a Pesin-like identity between the map's Lyapunov exponent and the graph's block entropy suggest that a graph analog of the Lyapunov exponent may be defined in network space [27].

IV. GRAPH-THEORETICAL RENORMALIZATION-GROUP ANALYSIS

Once the characteristic scalings of type-I intermittency have been recovered in the topology of the asssociated graphs, let us provide a wider picture of the phenomenon. The overall properties of intermittency graphs can be framed in the context of a renormalization-group (RG) transformation by following the procedure of previous studies [24–26]. We define an RG transformation $\mathcal{R}$ on an HV graph G as the coarse graining of every couple of adjacent nodes, where at least one of them has degree $k = 2$, into a block node that inherits the links of the previous two nodes. Iterating $\mathcal{R}$ we can trace the RG flows of intermittent graphs $G(\epsilon)$. Results include the following.

(i) When $\epsilon < 0$ ($\mu \gtrsim \mu_c$) trajectories are periodic and every HV graph trivially renormalizes towards the so-called chain graph G_0, an infinite chain with $k = 2$ for all nodes [24,25]. G_0 is invariant under renormalization $\mathcal{R}\{G_0\} = G_0$, and indeed constitutes a trivial (attractive) fixed point of the RG flow, $\mathcal{R}^{(n)}\{G(\epsilon < 0)\} = G_0$.

(ii) When $\epsilon > 0$ ($\mu \lesssim \mu_c$) repeated RG transformations eliminate progressively the links in the graph associated with correlations in the time series, leading ultimately to the HV graph that corresponds to a random time series. The links that stem from temporal correlated data connect primarily laminar nodes, whereas the links between either burst or peak nodes originate from uncorrelated segments of the time series. If the laminar episodes are eliminated from the time series, the burst and reinjection data values form a new time series that upon renormalization leads to the random time series. We have $\lim_{n\to\infty} \mathcal{R}^{(n)}\{G(\epsilon > 0)\} = G_{\text{rand}}$, where G_{rand} is the HVg associated with a random uncorrelated process with known graph properties [25]. This constitutes the second (attractive) fixed point of the RG flow.

(iii) At $\epsilon = 0$ ($\mu = \mu_c$) the HV graph generated by trajectories at tangency converges after only two steps of the RG transformation to a nontrivial fixed point $\mathcal{R}^2\{G(\epsilon = 0)\} = G_c = \mathcal{R}\{G_c\}$ and remains invariant under $\mathcal{R}$ afterwards. This feature can be demonstrated by explicit application of $\mathcal{R}$ upon $G(\epsilon = 0)$ (see Fig. 7 for a graphical illustration of this process). The fixed-point graph G_c is the HVg of a monotonically decreasing time series bounded at infinity by a large value; G_c is unstable under perturbations in ϵ and it is thus technically a saddle point of the RG flow, attractive along the critical manifold [spanned by $G(\epsilon = 0)$ and its replicas within other

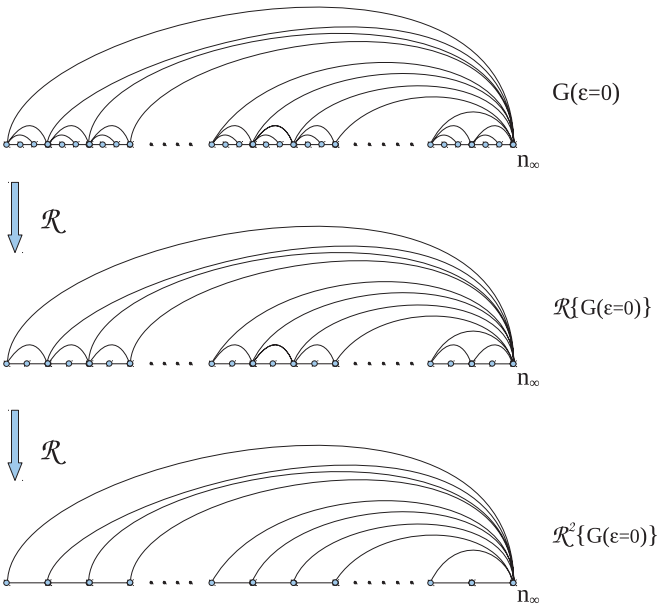

FIG. 7. (Color online) Illustration of the renormalization operator $\mathcal{R}$ applied on the HV graph at $\epsilon = 0$. This graph renormalizes, after two iterations of $\mathcal{R}$, into an HV graph G_c which is itself (i) invariant under $\mathcal{R}$, and (ii) unstable under perturbations in ϵ, thus constituting a nontrivial (saddle) fixed point of the graph-theoretical RG flow.

periodic windows of period T]. The RG flow diagram is shown in Fig. 8.

From visual inspection of Fig. 7 the degree distribution for $G(\epsilon = 0)$ is by construction

$$P(k;0) = \lim_{N\to\infty} \begin{cases} \frac{N/3}{N} & \text{if} \quad k = 2,3, \\ \frac{(N/3)-1}{N} & \text{if} \quad k = 6, \\ \frac{1}{N} & \text{if} \quad k = N/3, \end{cases} \tag{11}$$

and zero otherwise, where N is the number of nodes. Note that this expression coincides with the one predicted from our phenomenological theory when $\epsilon \to 0$. Its first moment is $\langle k\rangle = 4$, while its second moment $\langle k^2\rangle$ diverges, as expected from the previous result $\sigma_k^2 \sim \epsilon^{-0.5}$. By construction the degree distribution of G_c is

$$P_{G_c}(k) = \lim_{N\to\infty} \begin{cases} \frac{N-2}{N} & \text{if} \quad k = 3, \\ \frac{1}{N} & \text{if} \quad k = 2, \\ \frac{1}{N} & \text{if} \quad k = N-1, \end{cases} \tag{12}$$

and zero otherwise. The mean degree is again $\langle k\rangle = 4$ and its second moment also diverges.

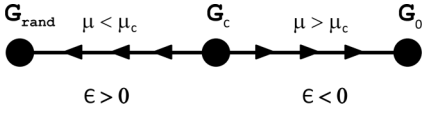

FIG. 8. Graph-theoretical RG flow of intermittent graphs. Graphs renormalize to G_0 for $\epsilon < 0$ and to G_{rand} for $\epsilon > 0$, the trivial (attractive) fixed points of the flow. The graph obtained at $\epsilon = 0$ renormalizes into G_c, which is invariant under the RG transformation and unstable under perturbations in ϵ, constituting the nontrivial graph-theoretical fixed point of the dynamics, whose degree distribution coincides with Eq. (12) for $\epsilon = 0$.

Let us return now, within our RG treatment, to the concept of graph-theoretical entropies h_n. We first look at the dependence of h_n on ϵ. This is shown when $\epsilon > 0$ in Fig. 6 in logarithmic scales and we observe that these functions are power laws that reach in every case a minimum at tangency. For concreteness we focus on h_1, for which $h_1(\epsilon = 0) = \log 3$. This minimum value of h_1 is retained for all $\epsilon < 0$ (but with $|\epsilon|$ below the period-doubling bifurcations that take place within the window of period 3). Hence entropy reaches a global minimum for the HV graph at tangency $\epsilon = 0$. Next we enquire about the effect of the RG transformations on h_1. The entropy at the nontrivial fixed point vanishes, as $h_1[P_{G_c}(k)] \to 0$ when $N \to \infty$, that is, the RG reduces h_1 when $\epsilon = 0$. Also, the RG transformations increase h_1 when $\epsilon > 0$ (as $h_1[P_{G_{\text{rand}}}(k)] = \log(27/4)$ [24,25]) and reduce it when $\epsilon < 0$ (since $h_1[P_{G_0}(k)] = 0$ [24,25]). When $\epsilon > 0$ the renormalization process of removal at each stage of all nodes with $k = 2$ eliminates node-node correlations (temporal correlations of the intermittent dynamics) and leads to a limiting renormalized system that consists only of a collection of uncorrelated variables, generating an irreversible flow along which the entropy grows. On the other hand, when $\epsilon < 0$ renormalization increments the fraction of nodes with degree $k = 2$ at each stage driving the graph structure towards the simple chain G_0 and thus decreases its entropy to its minimum value. Thus we observe the familiar picture of the RG treatment of a model phase transition, two trivial fixed points that represent disordered and ordered, or high- and low-temperature, phases, and a nontrivial fixed point with scale-invariant properties that represents the critical point. There is only one relevant variable, $\epsilon = \mu_c - \mu$, that is necessary to vanish to enable the RG transformation to access the nontrivial fixed point. The property that is seldom observed [34] is that an entropy functional, in the present case $h_1[P(k;\epsilon)]$, varies monotonously along the RG flows and is extremal at the fixed points. A salient feature of the HV studies of the routes to chaos in low-dimensional nonlinear iterated maps, period doubling [24,25], quasiperiodicity [26], and intermittency as presented here, is the demonstration that the entropy functional $h_1[P(k)]$ behaves as mentioned and attains extremal (maxima, minima, or saddle-point) values at the RG fixed points.

V. SUMMARY

We have demonstrated the capability of the HV algorithm for transforming into network language the properties of the route to chaos via intermittency of type I as it occurs in unimodal one-dimensional iterated maps. The outcome is a type of network architecture composed by nodes of three types with characteristic connectivities and that are the building blocks with which intermittency is expressed recursively via concatenation in network space. These node types arise from the laminar trends, the chaotic bursts, and the interfacial positions related to reinjection into the channel. Their relative numbers as a function of the channel width ϵ and their contributions to the degree distribution $P(k)$ were determined from a phenomenological theory, with accurate results in agreement with numerical simulations. We have shown that the characteristic ingredients of type-I intermittency are inherited

by the graph as functionals of the latter degree distribution, namely (i) the graph analog of the laminar phase mean length, which evidences the well-known scaling $\langle \ell \rangle \sim \epsilon^{-0.5}$, was identified to be the variance of the total degree distribution, and (ii) the Shannon block entropy over the degree distribution appears as the graph analog of the Lyapunov exponent λ, as the characteristic scaling $\lambda \sim \epsilon^{-0.5}$ is asymptotically recovered in network space through graph-theoretical block entropies h_n. We note at this point that Pesin identity suggests that a graph-theoretical analog to the Lyapunov exponents could be defined in the network context [27]. We also would like to highlight that while we have focused, for definiteness, in the logistic map close to the periodic window of period 3, results can be trivially extended to the intermittent dynamics close to any given periodic window or any chaotic map undergoing an inverse tangent bifurcation.

Significantly, the HV formalism leads to analytical expressions for the degree distribution near and at tangency. The scaling properties of the intermittent networks can be determined in terms of the same RG transformation employed with success on the HV graphs obtained for the period doubling and quasiperiodicity routes to chaos [24–26]. The graph-theoretical RG fixed points capture the features of the dynamics above, below, and at the tangent bifurcation. Finally, the optimization of a graph entropy introduced via the degree distribution reproduces the RG flows and fixed points.

In conclusion, the transition to chaos via type-I intermittency, as exemplified in unimodal maps near and at an inverse tangent bifurcation, has been fully described within the horizontal visibility theory. This technique may be extended to the study of other types of intermittency and may be useful for the analysis and interpretation of time series with sporadic features of diverse origin.

ACKNOWLEDGMENTS

We acknowledge financial support by the MEC and Comunidad de Madrid (Spain) through Projects No. FIS2009-13690 and No. S2009ESP-1691 (A.N., B.L., and L.L.), and support from CONACyT CB-2011-01-167978 & DGAPA (PAPIIT IN100311)-UNAM (Mexican agencies) (A.R.).

APPENDIX

Some properties of HV graphs which are relevant to the characteristics of intermittent series include the following.

(i) Drift. Let $\{x_i\}_{i=1,2,\ldots}$ be a monotonically increasing-decreasing series and define its drift as $\{d_i\}_{i=1,2,\ldots} \equiv \{x_{i+1} - x_i\}_{i=1,2,\ldots}$. Every node i of its HVg is connected only to the previous node $i-1$ and to the following node $i+1$, as it is always true that $x_{i+1} \geqslant x_i \geqslant x_{i-1}$ or $x_{i+1} \leqslant x_i \leqslant x_{i-1}$. Therefore, every node has connectivity $k = 2$ and the degree distribution is $P(k = 2) = 1$.

(ii) Periodicity. Let $\{x_i\}_{i=1,2,\ldots}$ be a periodic series of period T so that $x_{i+T} = x_i$. Let $x_{\max}$ be $\max\{x_k\}_{k=i,\ldots,i+T}$. Its HVg consists of a repeated periodic motif of T nodes from node $i_{\max}$ corresponding to $x_{\max}$ to node $i_{\max} + T$ corresponding to $x_{\max+T} = x_{\max}$ [19].

(iii) Periodicity with drift. Let $\{x_i^d\}_{i=1,2,\ldots}$ be a drifted periodic series with drifted period T so that $x_{i+T}^d = x_i^d + d_i$. If the series satisfies $\mid x_{i+1}^d - x_i^d \mid > \mid d_i - d_{i+1} \mid$ for all i, the HV graphs associated to $\{x_i^d\}$ and to $\{x_i\}$ in (ii) are identical.

(iv) Chaoticity. Let $\{x_i\}_{i=1,2,\ldots}$ be a chaotic series. The degree distribution of its HVg has an exponential tail $P(k) \sim \exp(-\lambda k)$ with $\lambda \geqslant \ln(3/2)$; the specific value of λ depends on the chaotic process from which the series has been extracted from [18].

Also note that the initial period-3 cycle behaves as $x_2 = \mu_c x_1(1-x_1)$, $x_3 = \mu_c x_2(1-x_2)$, $x_1 = \mu_c x_3(1-x_3)$, and in the chaotic vicinity of this orbit we have

$$x_2^d = (\mu_c - \epsilon)x_1(1-x_1) = \mu_c x_1(1-x_1) - \epsilon[x_1(1-x_1)] = x_2 - \epsilon\mu_c^{-1}x_2, \tag{A1}$$

$$x_3^d = (\mu_c - \epsilon)x_2\big(1-\epsilon\mu_c^{-1}\big)\big[1 - x_2\big(1-\epsilon\mu_c^{-1}\big)\big] \approx x_3 - \epsilon\mu_c^{-1}\big(2x_3 - \mu_c x_2^2\big), \tag{A2}$$

$$x_1^d \approx x_1 - \epsilon\mu_c^{-1}\big(x_1 - 4\mu_c x_3^2 + 2\mu_c x_3 + 2\mu_c^2 x_3 x_2^2 - \mu_c^2 x_2^2\big), \tag{A3}$$

that can be seen to be a perturbed periodic orbit. If we consider the series $\{x_i^d\}_{i=1,2,\ldots}$ to be periodic with a drift, $x_{i+T}^d = x_i^d + d_i$, then according to condition (iii) above the periodic HVg remains invariant for pseudoperiodic orbits $\{x_i^d\}_{i=1,2,\ldots}$.

[1] H. G. Schuster and W. Just, *Deterministic Chaos. An Introduction* (Wiley-VCH, Weinheim, 2005).
[2] J. Maurer and A. Libchaber, J. Physique Lett. **41**, 515 (1980).
[3] Y. Pomeau, J. C. Roux, A. Rossi, S. Bachelart, and C. Vidal, J. Physique Lett. **42**, 271 (1981).
[4] P. Bergé, M. Dubois, P. Manneville, and Y. Pomeau, J. Physique Lett. **41**, 341 (1980).
[5] P. Manneville and Y. Pomeau, Commun. Math. Phys. **74**, 189 (1980).
[6] N. Platt, E. A. Spiegel, and C. Tresser, Phys. Rev. Lett. **70**, 279 (1993).
[7] A. E. Hramov, A. A. Koronovskii, M. K. Kurovskaya, and S. Boccaletti, Phys. Rev. Lett. **97**, 114101 (2006).
[8] L. Lacasa, B. Luque, F. Ballesteros, J. Luque, and J. C. Nuño, Proc. Natl. Acad. Sci. USA **105**, 4972 (2008).
[9] B. Luque, L. Lacasa, F. Ballesteros, and J. Luque, Phys. Rev. E **80**, 046103 (2009).
[10] A. Nuñez, L. Lacasa, J. P. Gomez, and B. Luque, in *New Frontiers in Graph Theory*, edited by Y. Zhang (InTech, New York, USA, 2012).
[11] J. Zhang and M. Small, Phys. Rev. Lett. **96**, 238701 (2006).
[12] F. Kyriakopoulos and S. Thurner, Lect. Notes in Comput. Sci. **4488**, 625 (2007).
[13] X. Xu, J. Zhang, and M. Small, Proc. Natl. Acad. Sci. USA **105**, 19601 (2008).

[14] R. V. Donner, Y. Zou, J. F. Donges, N. Marwan, and J. Kurths, New J. Phys. **12**, 033025 (2010).
[15] R. V. Donner *et al.*, Int. J. Bif. Chaos **21**, 1019 (2010).
[16] R. V. Donner *et al.*, Eur. Phys. J. B **84**, 653 (2011).
[17] A. S. L. O. Campanharo, M. I. Sirer, R. D. Malmgren, F. M. Ramos, and L. A. N. Amaral, PLoS ONE **6**, e23378 (2011).
[18] L. Lacasa and R. Toral, Phys. Rev. E **82**, 036120 (2010).
[19] L. Lacasa, A. Núñez, É. Roldán, J. M. R. Parrondo, and B. Luque, Eur. Phys. J. B **85**, 217 (2012).
[20] L. Lacasa, B. Luque, J. Luque, and J. C. Nuño, Europhys. Lett. **86**, 30001 (2009).
[21] J. B. Elsner, T. H. Jagger, and E. A. Fogarty, Geophys. Res. Lett. **36**, L16702 (2009).
[22] L. Telesca and M. Lovallo, Europhys. Lett. **97**, 5 (2012).
[23] R. V. Donner and J. F. Donges, Acta Geophys. Pol. **60**, 589 (2012).
[24] B. Luque, L. Lacasa, F. Ballesteros, and A. Robledo, PLoS ONE **6**, e22411 (2011).
[25] B. Luque, L. Lacasa, F. Ballesteros, and A. Robledo, Chaos **22**, 013109 (2012).
[26] B. Luque, A. Núñez, F. Ballesteros, and A. Robledo, J. Nonlinear Sci. **23**, 335 (2013).
[27] B. Luque, L. Lacasa, and A. Robledo, Phys. Lett. A **376**, 3625 (2012).
[28] A. Nuñez, L. Lacasa, E. Luque, J. P. Gómez, and B. Luque, Int. J. Bif. Chaos **22**, 1250160 (2012).
[29] C. M. Kim, O. J. Kwon, E. K. Lee, and H. Lee, Phys. Rev. Lett. **73**, 525 (1994).
[30] For controlled reinjections, this scaling is of the form $\langle \ell \rangle \sim \epsilon^{-1/2}$ for uniformly distributed reinjection probabilities below tangency, whereas the scaling breaks down in favor of a logarithmic dependence if such reinjection occurs within a small neighborhood of the tangency region. If the reinjection probability is δ distributed, the exponent of the dynamics is found again and rather generally to be $1/2$ if the distribution is located below and sufficiently far from tangency, whereas an $\epsilon^{-1/4}$ scaling is found if the reinjection is deterministically performed at tangency. Finally, reinjections above tangency generate trivial ϵ^0 scaling [29]. On the other hand, natural reinjection, such as in the case of the logistic map close to any window of periodicity, occurs due to the presence of homoclinic orbits that take trajectories that leave the channel to place them arbitrarily close to the entrance of it at later, unpredictable, times. In this case the reinjection probability $p_0(y)$ is not controlled by hand and the resulting distribution of laminar sizes is asymmetrically U shaped [33]. However, noncontrolled reinjection usually yields again the $\epsilon^{-0.5}$ scaling for the mean length of laminar phases.
[31] It is well known [1,33] that $P(\ell;\epsilon) = \epsilon p_0(y)(1 + \tan^2[\pi/2 - \sqrt{\epsilon} a \ell])$ [33], where $p_0(y)$ is the reinjection probability distribution and $a = \frac{1}{2} \frac{d^2 F^{(3)}(x)}{dx^2}|_{x^*,\mu_c} \frac{dF^{(3)}(x)}{d\mu}|_{x^*,\mu_c} = 68.5$, such that $\langle \ell \rangle = \frac{\pi \epsilon^{-0.5}}{2\sqrt{a}}$ for small values of ϵ.
[32] A. E. Hramov, A. A. Koronovskii, M. K. Kurovskaya, A. A. Ovchinikov, and S. Bocaletti, Phys. Rev. E **76**, 026206 (2007).
[33] K. Karamanos and G. Nicolis, Chaos Solitons Fractals **10**, 7 (1999).
[34] A. Robledo, Phys. Rev. Lett. **83**, 2289 (1999).